Tribol Lett (2017) 65:132
DOI 10.1007/s11249-017-0911-z

Nanoscale Wear Layers on Silicon Wafers Induced by Mechanical Chemical Grinding

Zhenyu Zhang[1] · Yuefeng Du[1] · Bo Wang[1] · Ziguang Wang[1] · Renke Kang[1] · Dongming Guo[1]

Received: 24 May 2017 / Accepted: 19 August 2017 / Published online: 2 September 2017

Abstract Two types of diamond wheel with a mesh size of 20,000 are developed. A novel approach for mechanical chemical grinding (MCG) is proposed using the diamond wheels developed. A wear layer of 56 nm in thickness is obtained on a silicon wafer, which is ground by the diamond wheel with ceria at a feed rate of 20 μm/min. It consists of an amorphous layer at the top and a damage crystalline layer beneath. The thickness of the wear layer is less than one third those ground using a conventional diamond wheel with a mesh size of 3000. Surface roughness R_a and peak-to-valley values keep basically constant at 1 and 9.8 nm, respectively, with increasing feed rates from 5 to 20 μm/min, which is ground by the diamond wheel with ceria. Nanoscale wear layers are obtained on Si wafers ground by MCG in high efficiency, which is different from the traditional diamond grinding with thick wear layers and chemical mechanical grinding with low efficiency. The ground Si wafers are bright and absent of cracks. MCG paves the way for the applications in semiconductor and electronics industries.

Keywords Silicon · Nanoscale · Wear · Transmission electron microscopy · Grinding

✉ Zhenyu Zhang
zzy@dlut.edu.cn

[1] Key Laboratory for Precision and Non-Traditional Machining Technology of Ministry of Education, Dalian University of Technology, Dalian 116024, China

1 Introduction

Silicon (Si) is ubiquitous in contemporary technology. It is the second most abundant element in the earth's crust, existing naturally within various oxygen-rich minerals [1]. Si is an essential ingredient of modern technology because of its wide use in electronic devices [1–4]. It is a mainstay of semiconductor technology due to the elemental abundance, relatively low costs, ease of doping with other elements, as well as a native oxide passivation layer [1]. Single crystal Si is used to manufacture more than 90% of the semiconductor devices [5]. They are the foundation of the electronics industry, which is the largest industry all over the world. Si wafers are widely used as the substrate of semiconductor devices.

Grinding is one of the most important methods in manufacturing Si wafers and in thinning the device wafers [6–10]. It has both advantages of high accuracy and efficiency to remove the wear layers left on Si wafers by wire sawing from an ingot. The wear layer is the defect on a single crystal, which is induced by grinding. It consists of an amorphous layer at the top and a damaged crystalline layer beneath. Less cost and time for the subsequent chemical mechanical polishing (CMP) is associated with a thinner wear layer. Therefore, it is significant to review the thickness of wear layers produced by grinding. Table 1 lists the thicknesses of wear layers and grinding parameters of diamond grinding and chemical mechanical grinding (CMG) [11–15]. The thicknesses of wear layers are 41,230, 7020, 170–215, and 160–180 nm, which is ground by diamond wheels with mesh sizes of 600, 2000, 3000, and 5000, respectively. Thicknesses of wear layers decrease greatly in one order of magnitude with increasing mesh sizes from 600, 2000, to 3000. However, the thickness of wear layers remains invariable with further increasing of mesh sizes

Table 1 Thicknesses of wear layers and grinding parameters of diamond grinding and CMG [11–15]

Mesh size	Diamond grinding				CMG	
	600 [11]	2000 [11]	3000 [12–14]	5000 [15]	3000 [12–14]	
Bond	Resin	Resin	Resin	Vitrified	Resin	Magnesium oxychloride
Rotation speed of wheel (rpm)	2400	2400	2399, 2400	1800	500, 700	499, 700
Rotation speed of work (rpm)	150	150	120, 130, 149	50	120, 130	130, 149
Feed rate (μm/min)	10	10	10, 20 [13]	10	1	1
Thickness of wear layer (nm)	41,230	7020	170 [12], 180–190 [13], 215 [14]	160–180	10–19 [12], 35 [14]	10 [14], 12–14 [13]

from 3000 to 5000. This explains why the diamond wheel with mesh size of 3000 is the most popular product in ultraprecision grinding of Si wafers. The feed rate of diamond wheels is usually 10 μm/min [11–15], as well as 20 μm/min in diamond grinding with a mesh size of 3000 [13]. To reduce the thickness of wear layers, CMG is proposed in grinding the Si wafers. The thicknesses of wear layers formed by CMG vary from 10 to 35 nm, as listed in Table 1, which is comparable to that of CMP. Nevertheless, soft abrasives are used in CMG, rather than the hardest diamond abrasives. This results in a feed rate of only 1 μm/min [12–14]. Considering the deformation of soft abrasives during grinding, the actual material removal rate of CMG is also similar to that of CMP. Therefor, it is a challenge to obtain nanoscale wear layers for diamond grinding in high efficiency at a feed rate of 10 μm/min, which is highly desirable for semiconductor devices and the electronics industry to save cost and time for subsequent CMP processes. CMP is the most expensive process in manufacturing Si wafers, in terms of the operation, transportation, storage, and final treatment of chemical reagents.

In this study, a novel approach of mechanical chemical grinding (MCG) is proposed. Two types of diamond wheel are developed. Nanoscale wear layers are obtained in diamond grinding with high efficiency. The grinding and wear mechanisms are investigated using scanning electron microscopy (SEM) equipped with energy dispersive spectroscopy (EDS), X-ray photoelectron spectroscopy (XPS), X-ray diffraction (XRD), Raman spectra, and high resolution transmission electron microscopy (HRTEM) equipped with selected area electron diffraction (SAED).

2 Experimental Details

Commercially available 6-inch Si wafers (Grinm Advanced Materials Co., Ltd.) were used as specimens. One surface of a Si wafer was polished by CMP, which is fixed on the vacuum chuck. The other side of a Si wafer was a corrosive surface, which was used for MCG. Two types of diamond wheel were developed, and are designated as M1 and C2 with magnesia and ceria, respectively, as listed in Table 2. The bond used in the two wheels was zinc oxide (ZnO). Diamond abrasives, bond, and additive powders were mixed uniformly at room temperature and then pressed into segments by isostatic compaction. A segment was 22 mm long, 5 mm wide, and 10 mm high. The segments were sintered and vitrified completely at temperatures varying from 780 to 800 °C. Forty-four segments were distributed uniformly and glued in a notch at the periphery of an aluminum (Al) alloy plate. The diameter of the Al alloy plate was 350 mm. The concentration of diamond in a wheel was 200, which is a volume content, equivalent to a volume fraction of 50%. The mesh size of two diamond wheels was 20,000.

MCG was performed on an ultraprecision grinder (Okamoto, VG401 MKII, Japan), as shown in Fig. 1 and especially in Fig. 1c. The grinder could feed vertically only, guaranteeing the grinding accuracy with two air spindles. Taking into account the truing efficiency and quality, two truing methods were employed, as listed in Table 3. A diamond wheel was firstly trued by a cast iron plate with free abrasives of silicon carbide (SiC), followed by an alumina plate with deionized water as coolant. After truing, MCG was conducted on the corrosive surfaces of Si wafers. The grinding parameters are listed in Table 3. The grinding speed of wheels was 40.3 m/s, and the feed rates were set at 5, 10, 15, and 20 μm/min, respectively.

The vitrified diamond segments and ground Si wafers were characterized using a field emission SEM (FEI, Quanta 200 FEG, the Netherlands) equipped with EDS and measured by XRD (Bruker AXS D8 Discover, Germany) with copper radiation, XPS (PHI Quantera II, Japan), and Raman spectra (Renishaw inVia Reflex, UK) excited by a green laser with a wavelength of 532 nm. TEM samples were prepared firstly by a dimple grinder (Gatan 656,

Table 2 Description of the two developed diamond wheels

Diamond wheel	Additive (wt%)	Diamond abrasive (wt%)	Bond of ZnO (wt%)
M1	MgO 25	50.2	24.8
C2	CeO_2 38.5	40	21.5

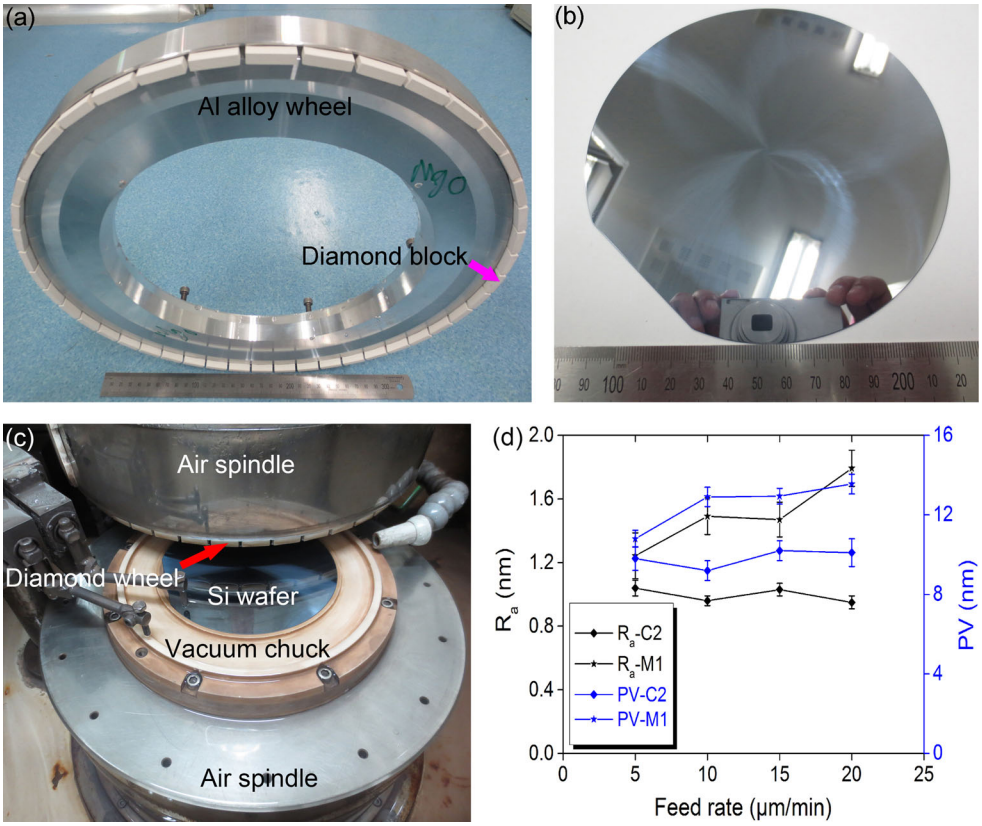

Fig. 1 Photographs of M1 (**a**), its ground Si wafer at a feed rate of 5 μm/min (**b**), and MCG on an ultraprecision grinder (**c**), and surface roughness (**d**) induced by two diamond wheels on ground Si wafers as a function of feed rate

Table 3 Grinding parameters of the two developed diamond wheels

Grinding parameter	Truing		MCG
Material of plate	Cast iron	Alumina	
Mesh of abrasive	400 (SiC)	2000	20,000
Rotation speed of wheel (rpm)	1500	1500	2199
Rotation speed of work (rpm)	5	10	100
Feed rate of wheel (μm/min)	3	3	5, 10, 15, 20
Diameter of wheel (mm)	350	350	350
Coolant of deionized water	Closed	Open	Open

USA), then polished by a disc grinder manually (Gatan 623, USA), and finally polished using a precision ion polishing system (Gatan 695, USA). TEM samples were characterized using an FEI Tecnai F20 at low magnification operated at 200 kV, and an FEI Titan G2 60-300 aberration corrected HRTEM at high magnification operated at 300 kV. Hardness and elastic modulus were measured by a nanomechanical tester (TI 950 TriboIndenter®, Hysitron, Minneapolis, MN, USA) at peak loads of 4, 5, and 6 N, respectively. Surface roughness R_a, root mean square (rms) and peak-to-valley (PV) values were measured by a non-contact precision surface profilometer (Zygo, NewView 5022, USA). The area was 71 × 53 μm^2 for each measurement of surface roughness.

3 Results

Figure 1 shows the photographs of M1, its ground Si wafer and MCG on an ultraprecision grinder, and surface roughness induced by two diamond wheels on ground Si wafers. A vitrified diamond wheel of M1 is developed, as illustrated in Fig. 1a. A ground Si water of M1 looks bright and like a mirror, pictured in Fig. 1b. M1 is mounted on an

ultraprecision grinder and a Si wafer is fixed on vacuum chuck, as shown in Fig. 1c. Surface roughness R_a and PV values of C2 are obvious lower than those of M1, as drawn in Fig. 1d. Surface roughness induced by two diamond wheels is listed in Table 4. The surface roughness R_a produced by M1 varies from 1.24 to 1.79 nm, with increasing feed rates from 5 to 20 μm/min, corresponding to the PV values changing from 10.8 to 13.5 nm.

Figure 2 illustrates the SEM images of M2 and its EDS, XRD, XPS, and Raman spectra. The surface of M2 is porous and looks uniform, as shown in Fig. 2a, b). The C element is the most up to 54.86 wt% (Fig. 2c), which is consistent with the highest peak of diamond in Fig. 2d. The weight percentages of Mg, Zn, and Si elements are 14.55, 12.2, and 1.35% (Fig. 2c), respectively. Diamond, MgO, ZnO, zinc carbonate ($ZnCO_3$), SiO_2, and SiC are confirmed by XRD in Fig. 2d. ZnO, MgO, and SiC are identified by XPS in Fig. 2e at 1021.7, 88 and 100.9 eV, respectively [16, 17]. A sharp diamond peak is present at 1332 cm^{-1} [18] (Fig. 2f), and a broad amorphous peak centered at 1430 cm^{-1} is the characteristics of amorphous carbon (a–C), deriving from the diamond abrasives [19, 20].

Figure 3 pictures SEM images of ground Si wafers of M1 at feed rates of 5 and 20 μm/min. All the ground surfaces have wear tracks, without cracks, indicating ductile grinding characteristics. Moreover, the ground surface in Fig. 3d is smeared, meaning the alleviative grinding.

Figure 4 shows the representative EDS, XRD, XPS, and Raman spectra on ground Si wafers of M1 at a feed rate of 5 μm/min. A Si peak is found by EDS in Fig. 4a. SiO_2 peaks are confirmed by XRD in Fig. 4b. Si and SiO_x peaks are identified by XPS spectra in Fig. 4c at 98.4 and 102.2 eV, respectively [16, 17]. A sharp Si peak is determined by Raman spectrum in Fig. 4d at 520 cm^{-1} [21]. Hereby, Si, SiO_2 , and SiO_x are identified by EDS, XRD, XPS, and Raman spectra, verifying the clean grinding of M1 and without contaminants generated by M1.

Figure 5 illustrates the cross-sectional TEM images of a ground Si wafer by M1 at a feed rate of 5 μm/min. The wear layer is 94 nm in thickness, consisting of an amorphous layer at the top, followed by a damage crystalline layer underneath (Fig. 5a). It is interesting that the nanoscale wear layer induced by M1 is obtained. The SAED pattern illustrates the pristine Si-I phase, absent of high pressure phases, as seen in the *inset* of Fig. 5a. In Fig. 5b, the distances between crystalline planes are different, indicating the formation of crystallites.

Figure 6 shows the truing of C2 mounted on an ultraprecision grinder and its ground Si wafer. The developed diamond wheel C2 is trued by a green alumina plate, which is fixed by vacuum chuck of an ultraprecision grinder, as diagramed in Fig. 6a. A ground Si wafer of C2 looks bright and like a mirror, as illustrated in Fig. 6b.

Figure 7 shows the SEM images of C2 and its EDS, XRD, XPS, and Raman spectra in (a). The surface of vitrified diamond wheel C2 is porous, as illustrated in Fig. 7a, b. C2 consists of C, O, Mg, Si, Ce, Zn elements with weight percentages of 13.98, 3.17, 1.65, 1.99, 64.09, 15.12%, respectively, as listed by EDS in Fig. 7c. Sharp peaks of CO_2 are identified by XRD in Fig. 7d, whose intensities are stronger than those of diamond. Only CeO_2 and diamond crystalline peaks are found in XRD of C2, exhibiting the perfect vitrified effect of C2, compared with M1. ZnO peaks are determined by XPS in Fig. 7e at 10.3, 89, 140, and 1022 eV for Zn 3d, Zn $3p_{3/2}$, Zn 3s, and Zn $2p_{3/2}$, respectively [17]. SiC peaks are identified at 101.5 and 151.3 eV for Si $2p_{3/2}$ and Si 2 s, respectively. CeO_2 peak is found at 882.9 eV for Ce $3d_{5/2}$ [17]. Sharp CeO_2 and diamond peaks are found by Raman spectra in Fig. 7f at 466 [22] and 1332 [18] cm^{-1} respectively, and the intensity of the former is stronger than that of the latter. This is consistent with the results of XRD in Fig. 7d. A broad peak centered at 1430 cm^{-1} corresponds to the a–C, which is derived from the diamond abrasives [19, 20].

Table 4 Surface roughness and calculated undeformed chip thickness induced by the two developed diamond wheels

Diamond wheel	Feed rate of wheel (μm/min)	Surface roughness (nm)		Calculated undeformed chip thickness (nm)
		R_a	PV	
M1	5	1.24 ± 0.14	10.8 ± 0.4	0.49
	10	1.5 ± 0.12	12.9 ± 0.5	0.69
	15	1.47 ± 0.11	12.9 ± 0.4	0.85
	20	1.79 ± 0.11	13.5 ± 0.5	0.98
C2	5	1.04 ± 0.05	9.8 ± 0.6	0.6
	10	0.96 ± 0.03	9.2 ± 0.5	0.86
	15	1.03 ± 0.04	10.2 ± 0.5	1.05
	20	0.95 ± 0.04	10.1 ± 0.7	1.21

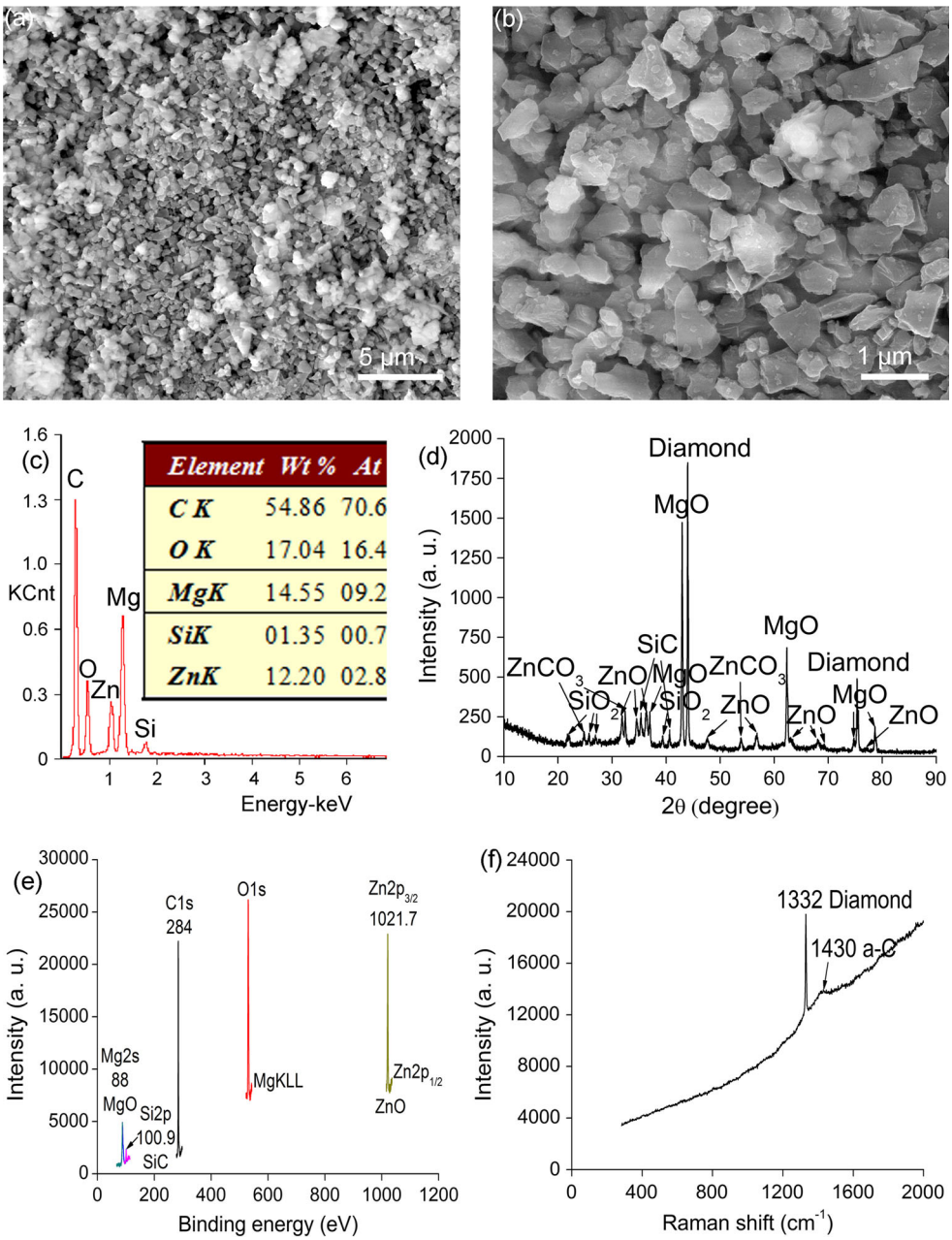

Fig. 2 SEM images of M2 at low (**a**) and high (**b**) magnifications and its EDS (**c**), XRD (**d**), XPS (**e**), and Raman (**f**) spectra in (**a**)

Figure 8 pictures the SEM images of Si wafers ground by C2 at feed rates of 5 and 20 μm/min. There are no cracks and sharp wear tracks on all the ground Si wafers, indicating the characteristics of mild and ductile grinding. This is in a good agreement with the ground Si wafers of M1 in Fig. 3. The surface roughness R_a and PV values ground by C2 keeps basically constants at 1 and 9.8 nm, respectively, with increasing feed rates from 5 to 20 μm/min, as listed in Table 4 and illustrated in Fig. 1d. The surface roughness R_a and PV values are 0.95 and 10.1 nm, respectively, on Si wafers ground by C2 at a feed rate of 20 μm/min, indicating ultra-smooth surfaces obtained in high efficiency.

Figure 9 diagrams the representative EDS, XRD, XPS, and Raman spectra on Si wafers ground by C2 at a feed rate of 20 μm/min. Si and SiO_2 are ascertained by EDS and XRD, respectively, corresponding to Fig. 9a, b. Si and SiO_x are identified at 98.6 and 102.3 eV, respectively, in Fig. 9c, which corresponds to Si 2p [16, 17]. A sharp Si peak is confirmed by Raman spectra at 520 cm^{-1} in Fig. 9d [21]. Si, SiO_2 and SiO_x are found by EDS, XRD, XPS, and Raman spectra, displaying the clean grinding, without contaminants from the diamond wheel of C2. This agrees well with the experimental results of M1 in Fig. 4.

Figure 10 illustrates the cross-sectional TEM images of a ground Si wafer by C2 at a feed rate of 20 μm/min. The

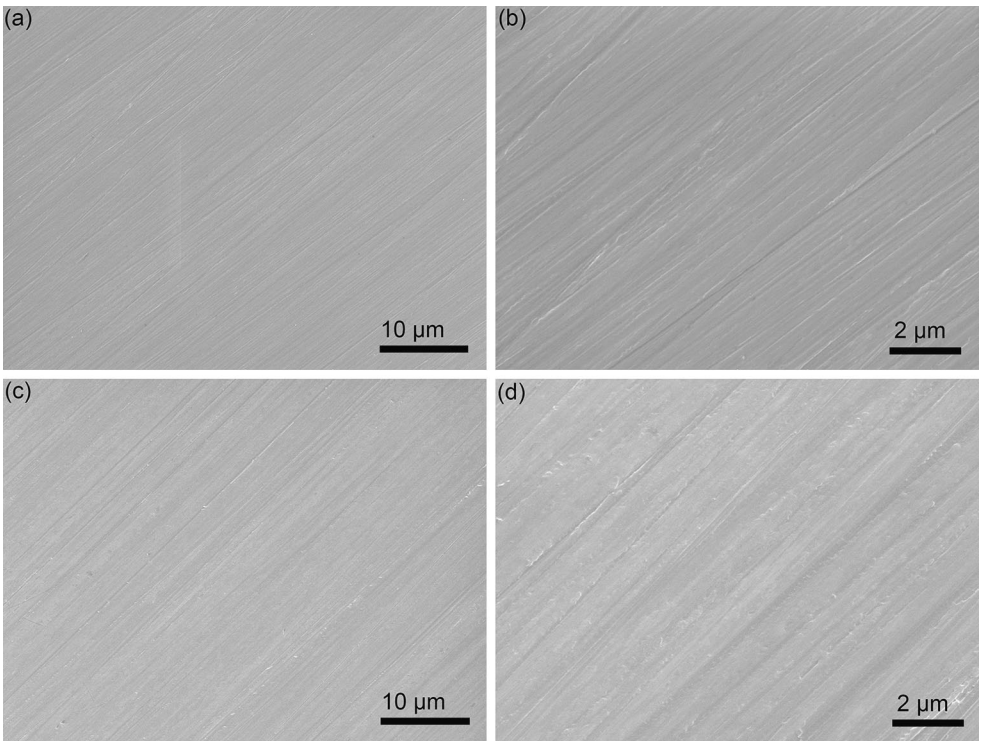

Fig. 3 SEM images of ground Si wafers of M1 at feed rates of 5 (**a**), (**b**) and 20 (**c**), (**d**) μm/min at low (**a**), (**c**) and high (**b**), (**d**) magnifications

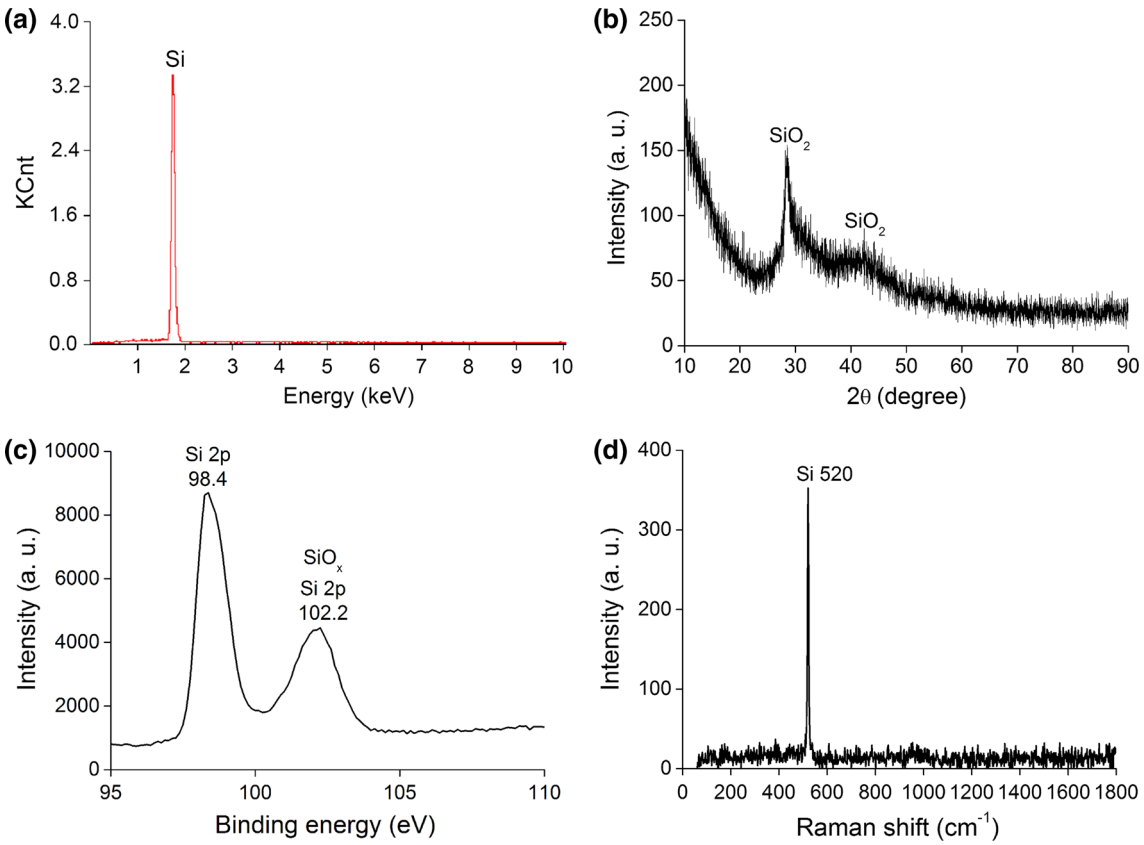

Fig. 4 EDS (**a**), XRD (**b**), XPS (**c**), and Raman spectra (**d**) on ground Si wafers of M1 at a feed rate of 5 μm/min

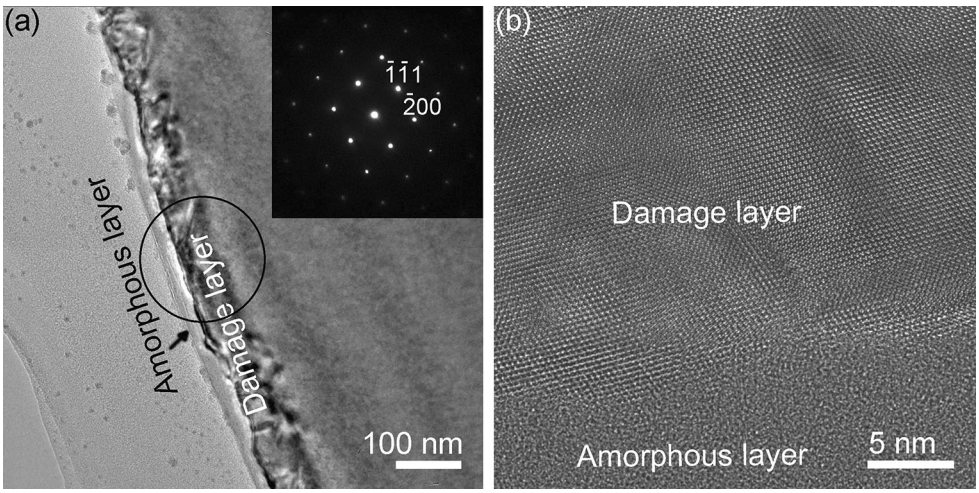

Fig. 5 Cross-sectional TEM images of a ground Si wafer by M1 at a feed rate of 5 μm/min at low (**a**) and high (**b**) magnifications. *Inset* showing its corresponding SAED pattern marked in a *black circle* in (**a**)

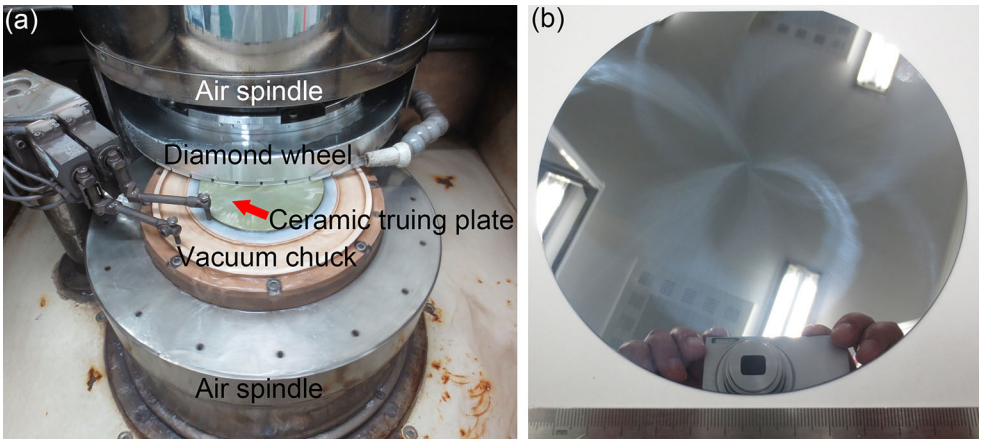

Fig. 6 Photographs for truing of C2 (**a**) mounted on an ultraprecision grinder and its ground Si wafer (**b**)

SAED pattern exhibits the pristine Si-I phase, without high pressure phases, as found in the inset of Fig. 10a. The wear layer of 56 nm in thickness consists of an amorphous layer at the top and a damage crystalline layer beneath, as shown in Fig. 10a, which is less than one third that ground by a conventional diamond wheel with a mesh size of 3000 [12–14]. Crystal lattice of damage crystalline layer is shown in Fig. 10b, and the distances between crystalline places are different, indicating the generation of crystallites.

4 Discussion

The maximum undeformed chip thickness, h_m can be used to characterize the grinding conditions [23–25]. h_m is significant for the grinding performance and processing. Usually, the smaller the h_m, the thinner of wear layers ground by diamond wheels, and the lower surface roughness. It is calculated [24, 25],

$$h_m = \frac{E_1}{E_2}\left(\frac{4}{rC^{1.5}}\frac{v_f}{v_s}\right)^{0.5} \quad (1)$$

where, E_1 and E_2 are the elastic moduli of diamond wheels and specimens, respectively, r is the ratio of width to thickness of an undeformed chip, C is the quantity of surface active grains per unit area, and v_f and v_s are the feed rates of the diamond wheel and grinding speed, respectively. Figure 11 draws the hardness and elastic modulus of the two developed diamond wheels as a function of load. The hardness of M1 and C2 is approximately 178 and 600 MPa respectively, as shown in Fig. 11a. This is because of the porous structure on the surfaces of two vitrified diamond wheels. The elastic moduli of M1 and C2 are 30.8 and 38.1 GPa, respectively, as illustrated in Fig. 11b. r is 1.49 [25]. C is expressed [24, 25],

$$C = \frac{4f}{d_g^2\left(\frac{4\pi}{3v}\right)^{2/3}} \quad (2)$$

where f is the ratio of active grains to the total ones on the

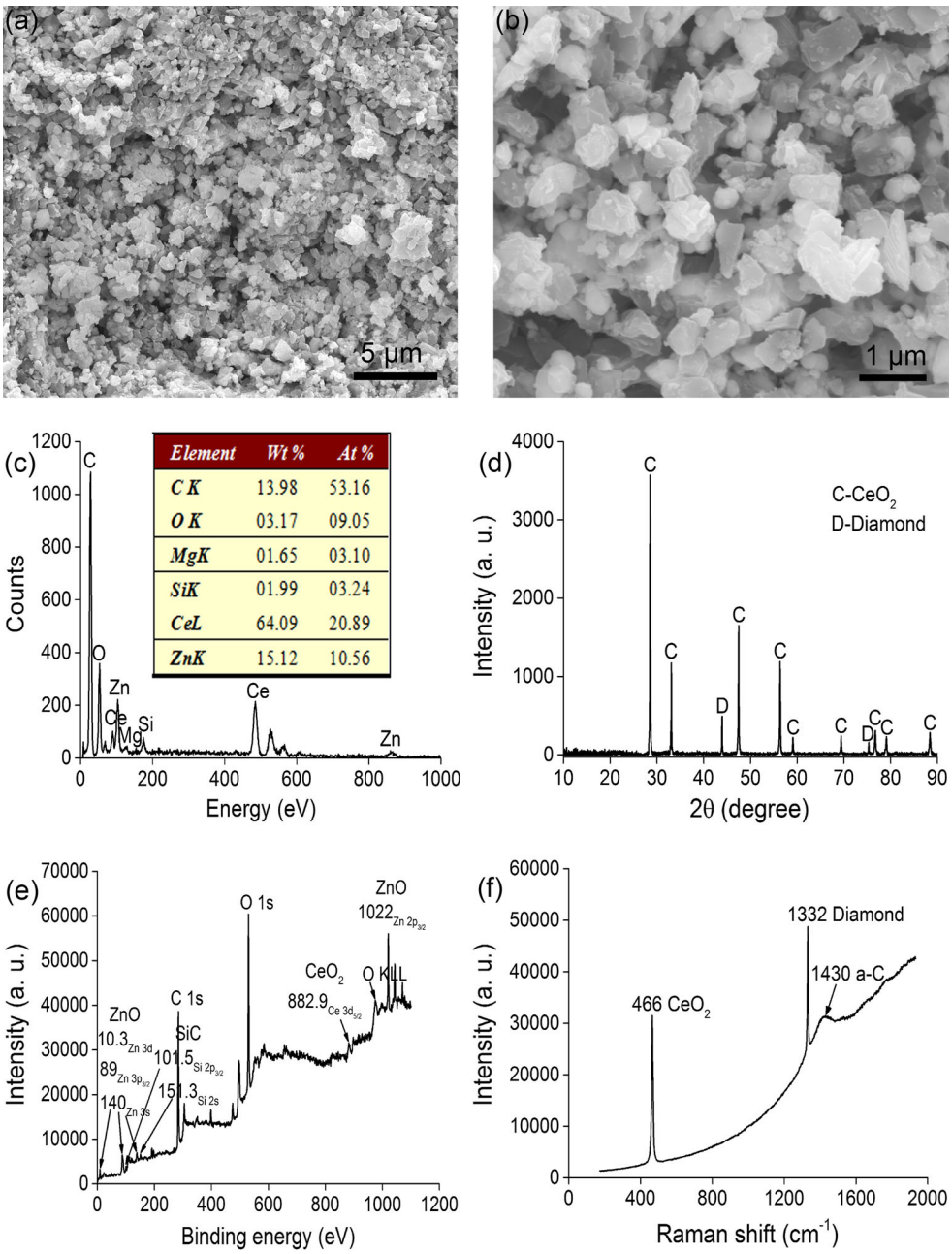

Fig. 7 SEM images of C2 at low (**a**) and high (**b**) magnifications and its EDS (**c**), XRD (**d**), XPS (**e**), and Raman spectra (**f**) in (**a**)

surface, d_g is the equivalent diameter of grains, and v is the volume fraction of diamond grains. f is 0.5 in grinding [26]. d_g is presented [27],

$$d_g(\text{mm}) = \frac{15.2}{M} \tag{3}$$

where M is the mesh size of a diamond wheel. d_g is 760 nm for the two diamond wheels with a mesh size of 20,000. h_m is listed in Table 4. It increases monotonously from 0.49 to 0.98 nm and from 0.6 to 1.21 nm for M1 and C2, respectively, with increasing feed rates from 5 to 20 μm/min. All values of h_m for M1 and C2 are less than 1.3 nm, which is very small, contributing greatly to the nanoscale wear layers on Si wafers, as illustrated in Figs. 5 and 10, as well as for lower surface roughness listed in Table 4. Nevertheless, the surface roughness and wear layer ground by C2 are much smaller than those of M1, at the same grinding parameters and mesh sizes of grains for the two diamond wheels. This is attributed to the different MCG effects of M1 and C2 on Si wafers.

M1 consists of diamond, ZnO and MgO in majority, and a bit of SiC and SiO_2, as illustrated in Fig. 2. $ZnCO_3$ is formed during sintering, benefiting for the generation of porous structure in the vitrified diamond wheel. C2 includes mainly diamond, ZnO and CeO_2, and a few SiC,

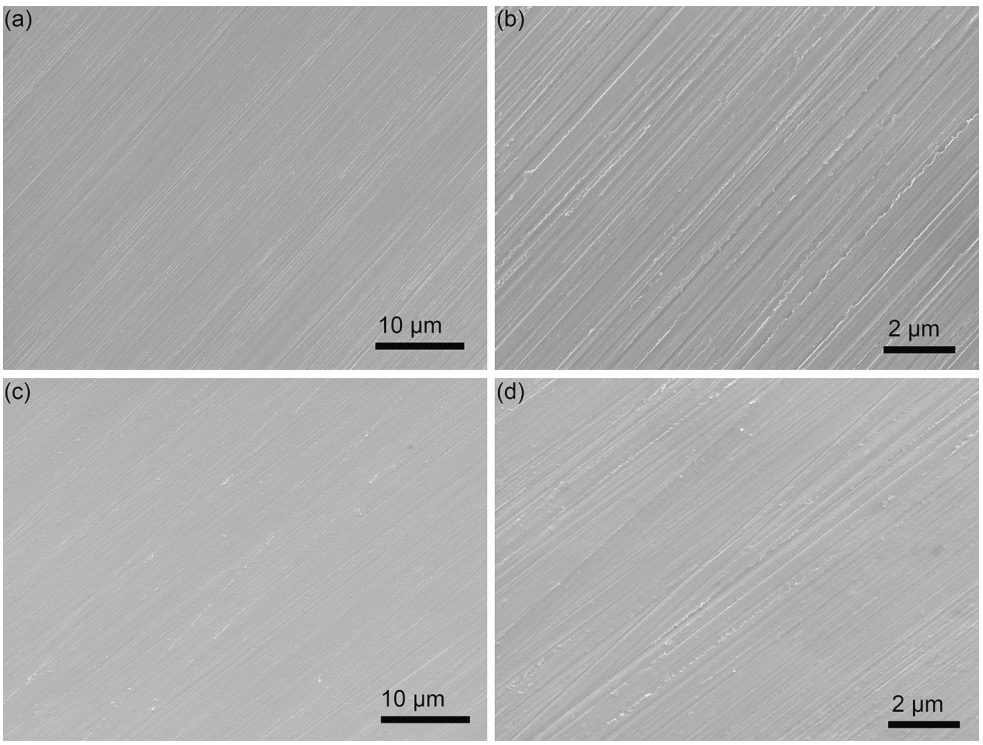

Fig. 8 SEM images of Si wafers ground by C2 at feed rates of 5 (**a**), (**b**) and 20 (**c**), (**d**) μm/min at low (**a**), (**c**) and high (**b**), (**d**) magnifications

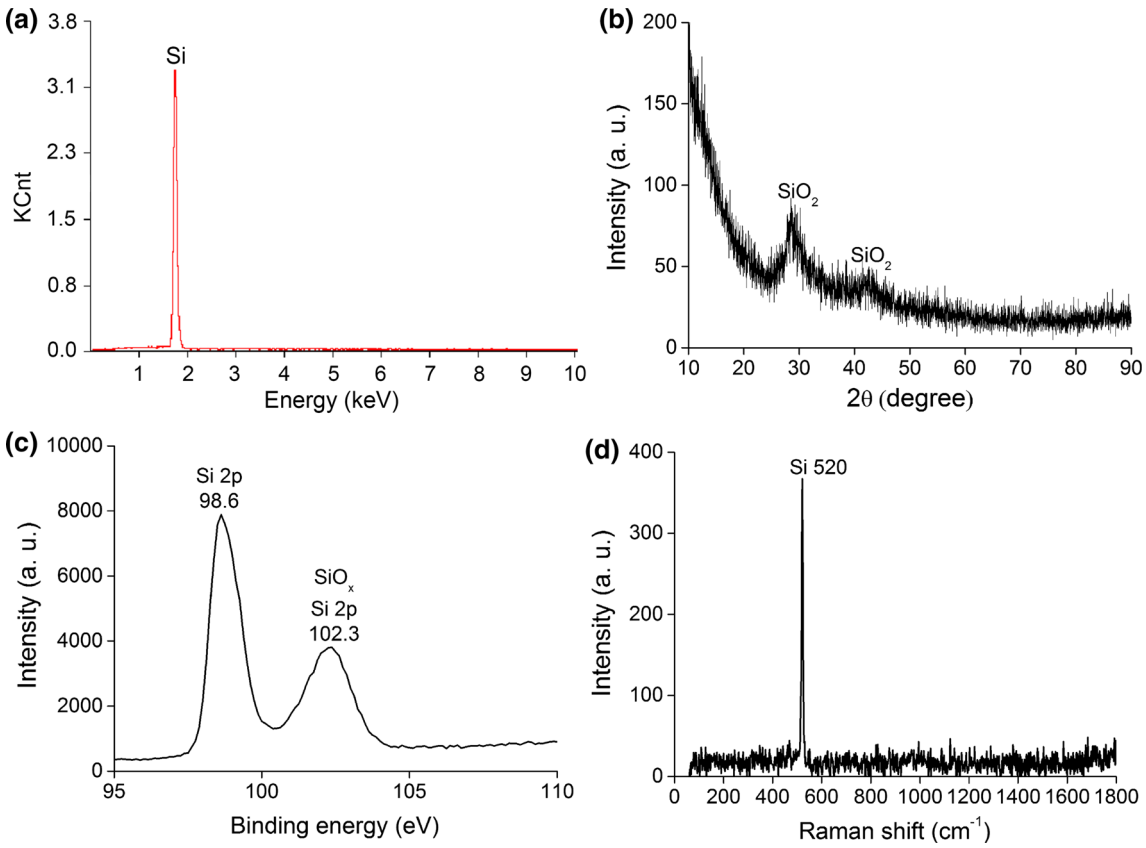

Fig. 9 EDS (**a**), XRD (**b**), XPS (**c**), and Raman spectra (**d**) on ground Si wafers of C2 at a feed rate of 20 μm/min

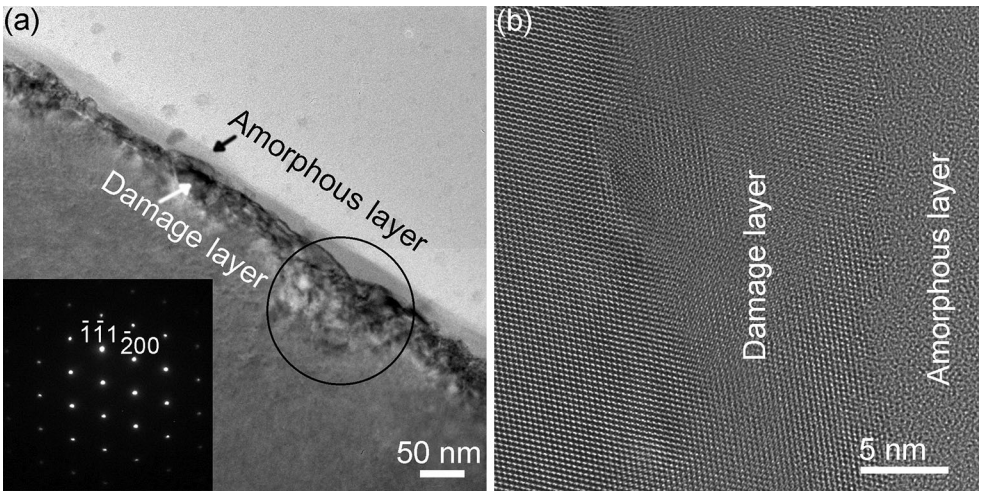

Fig. 10 Cross-sectional TEM images of a ground Si wafer by C2 at a feed rate of 20 μm/min at low (**a**) and high (**b**) magnifications. *Inset* showing its corresponding SAED pattern marked in a *black circle* in (**a**)

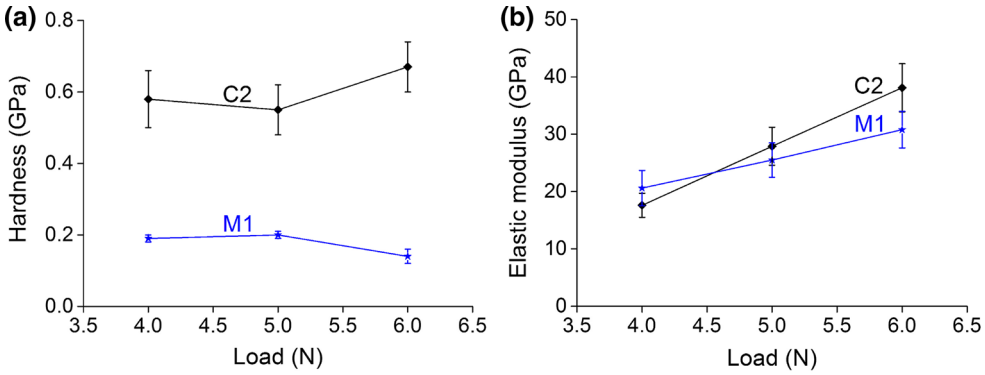

Fig. 11 Hardness (**a**) and elastic modulus (**b**) of the two developed diamond wheels as a function of load

as pictured in Fig. 7. ZnO is the bond in both M1 and C2. In developing a new diamond wheel, two types of ceramics are appropriate during sintering to control the temperature. Two ceramics are insensitive for a small variation of temperature, facilitating the formation of vitrified diamond wheel. Thus, both M1 and C2 consist of two main ceramics, in addition to diamond grains. Some additives of ceramics are beneficial for the production of porous structure in the two vitrified diamond wheels, due to the different volume shrinkage of ceramics during sintering [23]. MgO and CeO_2 are responsible for the MCG effects in M1 and C2, respectively.

ZnO is used to decrease the dissolution rate of the vitrified block made of diamond wheels, increasing their lifetime [28]. During sintering, non-bridging oxygen is created within the vitrified bond of ZnO, strengthening the interfacial bonding between diamond grains and bond [29]. Furthermore, the oxidation resistance of diamond grains is increased under the protection of ZnO, enhancing the bending strength of vitrified blocks composed of two diamond wheels [30]. Consequently, ZnO is selected as the bond of two developed diamond wheels, for obtaining good grinding performance.

SiC is used in both diamond wheels of M1 and C2. It exhibits high thermal conductivity [31], low thermal expansion, low fracture toughness, chemical inertness at elevated temperature, high hardness and wear resistance, and low density [23, 32]. In M1 and C2, the diamond grains are very small, and their equivalent diameter is 760 nm. For this reason, SiC participates in grinding, especially when diamond grains are worn and pulled out. Moreover, it can take away the grinding heat immediately induced by grinding, because of its high thermal conductivity. This is because SiC has a ratio of 9:1 of covalent to ionic bonding [33]. On the other hand, SiC and SiO_2 can bond well [34]. Hence, SiC and SiO_2 are both added in M1. Furthermore, SiO_2 promotes the uniform distribution of vitrified amorphous phase, decreases the melting temperature and reduces the nucleation of crystalline phases during sintering [35].

CeO_2 and MgO are stable in air. However, a Si wafer is exposed in air, as explained in the following equation,

$$Si + O_2 \rightarrow SiO_2 \quad (4)$$

During grinding, the air is insufficient at the grinding zone, as shown in Eq. 5,

$$2Si + xO_2 \rightarrow 2SiO_x \quad (5)$$

CeO_2 and MgO do not react with SiO_2 at room temperature. They can react with SiO_2 under stress induced by grinding firstly, followed by the united effects of mechanical force and heat generated by friction during grinding. Moreover, diamond grinding happens in both M1 and C2 to remove the material of workpiece in high efficiency, which is different from CMG in a low material removal rate. Wherefore, a novel approach of MCG is proposed. The reactions between MgO and Si or SiO_2 are as follows,

$$Si + O_2 + MgO \rightarrow MgSiO_3 \quad (6)$$

$$MgO + SiO_2 \rightarrow MgSiO_3 \quad (7)$$

These two equations are activated by the mechanical force firstly, and then by the combined effects of mechanical force and grinding heat induced by grinding. The MCG of M1 alleviates the aggressive grinding taken place in traditional diamond grinding, and wild ground surfaces are observed in Fig. 3. Under the MCG effect, the smeared surface ground by M1 is found in Fig. 3c, and a wear layer of 94 nm in thickness is produced by grinding in Fig. 5a. Thus, the nanoscale wear layer is obtained.

Compared with MgO, CeO_2 has unique mechanical and chemical characteristics. For instance, it has high thermal stability, in terms of a melting point up to 2400 °C [36]. This means that CeO_2 is in a perfect crystalline phase during sintering, as illustrated in Fig. 7(d). As an ultrathin SiO_2 layer is formed on a Si wafer exposed to air, grinding will remove the SiO_2 layer first. MCG begins from the mechanical force first. Under grinding, a mechanical force is applied on the Si wafers, which makes the O bonds of SiO_2 broken. This triggers the reduction reactions of CeO_2 from Ce^{4+} to Ce^{3+} under the coherent effects of mechanical force and grinding heat. Four equations are suggested in air and deionized water during grinding of C2 [37, 38],

$$4Ce^{4+} + Si^0 \rightarrow 4Ce^{3+} + Si^{4+} \quad (8)$$

$$Si + SiO_2 + 4CeO_2 \rightarrow 2Ce_2O_3 + 2SiO_2 \quad (9)$$

$$4SiO_x + 3O_2 + 4CeO_2 \rightarrow 2Ce_2O_3 + 2xO_2 + 4SiO_2 \quad (10)$$

$$4CeO_2 + 6H_2O \rightarrow 4Ce(OH)_3 + O_2 \quad (11)$$

The reduction reactions lead to the transfer of electrons from the *p*-orbital of O atoms to the *f*-orbital of Ce atoms, forming the Si–O–Ce bonding with the dangling bonds of O atoms [39]. With the formation of Si–O–Ce bonding, SiO_2 lump is pulled out and removed from the SiO_2 layer, under the combined effects of mechanical force and heat induced by grinding [39]. Si^{4+} and Ce^{3+} ions are easily removed at the forms of silicates and cerium hydroxide in deionized water, respectively. The reduction reactions of CeO_2 cause C2 to obtain a wear layer of 56 nm in thickness, as illustrated in Fig. 10a, as well as lower surface roughness compared to M1, as pictured in Fig. 1d. Nanoscale wear layer produced by C2 in high efficiency is consistent with previous reports, in which CeO_2 obtains the highest material removal rate in abrasive machining, compared with Al_2O_3, TiO_2, Y_2O_3, ZrO_2, SnO_2, Cr_2O_3, and La_2O_3 [40]. MCG of C2 starts from the mechanical force applied by grinding, followed by the united effects of mechanical force and grinding heat.

5 Conclusions

In summary, two types of diamond wheel are developed to perform MCG. M1 consists of diamond abrasives, ZnO and MgO in majority, and a bit of SiC and SiO_2. C2 includes diamond abrasives, ZnO and CeO_2 mainly, and a few SiC. The addition of CeO_2 makes C2 exhibit only two crystalline phases of CeO_2 and diamond, indicating perfect vitrified effect. Nanoscale wear layers are obtained on ground Si wafers by the two developed diamond wheels. Surface roughness R_a and PV values are stable on ground Si wafers by C2, with increasing feed rates from 5 to 20 μm/min. All the surface roughness R_a and PV values induced by C2 are lower than those of M1. Nanoscale wear layers in high efficiency are obtained on Si wafers in MCG of C2, which is attributed to the reduction reactions of CeO_2 under the combined effects of mechanical force and grinding heat. MCG has great potential applications in the fields of semiconductors, microelectronics, and optoelectronics.

Acknowledgements The authors acknowledge for the financial supports from the Excellent Young Scientists Fund of NSFC (51422502), Integrated Program for Major Research Plan of NSFC (91323302), Science Fund for Creative Research Groups of NSFC (51621064), Changjiang Scholars Program of Ministry of Education of China, the Xinghai Science Funds for Distinguished Young Scholars and Thousand Youth Talents at Dalian University of Technology, the Natural Science Foundation of Jiangsu Province (BK20151190), Distinguished Young Scholars for Science and Technology of Dalian City (2016RJ05), and the Collaborative Innovation Center of Major Machine Manufacturing in Liaoning.

References

1. Kim, D.Y., Stefanoski, S., Kurakevych, O.O., Strobel, T.A.: Synthesis of an open-framework allotrope of silicon. Nat. Mater. **14**(2), 169–173 (2015)
2. Kim, K., Choi, J.Y., Kim, T., Cho, S.H., Chung, H.J.: A role for graphene in silicon-based semiconductor devices. Nature **479**(7373), 338–344 (2011)

3. Mi, X., Cady, J.V., Zajac, D.M., Deelman, P.W., Petta, J.R.: Strong coupling of a single electron in silicon to a microwave photon. Science **355**(6321), 156–158 (2017)
4. Cassidy, M.C., Chan, H.R., Ross, B.D., Bhattacharya, P.K., Marcus, C.M.: In vivo magnetic resonance imaging of hyperpolarized silicon particles. Nat. Nanotechnol. **8**(5), 363–368 (2013)
5. Liu, J.H., Pei, Z.J., Fisher, G.R.: ELID grinding of silicon wafers: a literature review. Int. J. Mach. Tools Manuf **47**(3–4), 529–536 (2007)
6. Zhang, Z.Y., Guo, L.C., Cui, J.F., Wang, B., Kang, R.K., Guo, D.M.: Nanoscale solely amorphous layer in silicon wafers induced by a newly developed diamond wheel. Sci. Rep. **6**, 35269 (2016)
7. Zhang, Z.Y., Guo, D.M., Wang, B., Kang, R.K., Zhang, B.: A novel approach of high speed scratching on silicon wafers at nanoscale depths of cut. Sci. Rep. **5**, 16395 (2015)
8. Zhang, Z.Y., Wang, B., Kang, R.K., Zhang, B., Guo, D.M.: Changes in surface layer of silicon wafers from diamond scratching. CIRP Ann. Manuf. Technol. **64**(1), 349–352 (2015)
9. Ding, W.F., Xu, J.H., Chen, Z.Z., Yang, C.Y., Song, C.J., Fu, Y.C.: Fabrication and performance of porous metal-bonded CBN grinding wheels using alumina bubble particles as pore-forming agents. Int. J. Adv. Manuf. Technol. **67**(5–8), 1309–1315 (2013)
10. Dai, C.W., Ding, W.F., Xu, J.H., Fu, Y.C., Yu, T.Y.: Influence of grain wear on material removal behavior during grinding nickel-based superalloy with a single diamond grain. Int. J. Mach. Tools Manuf **113**, 49–58 (2017)
11. Gao, S., Dong, Z.G., Kang, R.K., Zhang, B., Guo, D.M.: Warping of silicon wafers subjected to back-grinding process. Precis. Eng. **40**, 87–93 (2015)
12. Gao, S., Dong, Z.G., Kang, R.K., Guo, D.M.: Design and evaluation of soft abrasive grinding wheels for silicon wafers. Proc. Inst. Mech. Eng. Part B J. Eng. Manuf. **227**(B4), 578–586 (2013)
13. Dong, Z.G., Gao, S., Huang, H., Kang, R.K., Wang, Z.G.: Surface integrity and removal mechanism of chemical mechanical grinding of silicon wafers using a newly developed wheel. Int. J. Adv. Manuf. Technol. **83**(5–8), 1231–1239 (2016)
14. Gao, S., Huang, H., Zhu, X.L., Kang, R.K.: Surface integrity and removal mechanism of silicon wafers in chemo-mechanical grinding using a newly developed soft abrasive grinding wheel. Mater. Sci. Semicond. Process. **63**, 97–106 (2017)
15. Huang, H., Wang, B.L., Wang, Y., Zou, J., Zhou, L.: Characteristics of silicon substrates fabricated using nanogrinding and chemo-mechanical-grinding. Mater. Sci. Eng., A **479**(1–2), 373–379 (2008)
16. Wagner, C.D., Riggs, W.M., Davis, L.E., Moulder, J.F., Muilenberg, G.E. (eds.): Handbook of X-ray Photoelectron Spectroscopy. Perkin-Elmer Corporation, Physical Electronics Division, Minnesota (1979)
17. https://srdata.nist.gov/xps/main_search_menu.aspx
18. Mohr, M., Daccache, L., Horvat, S., Bruhne, K., Jacob, T., Fecht, H.J.: Influence of grain boundaries on elasticity and thermal conductivity of nanocrystalline diamond films. Acta Mater. **122**, 92–98 (2017)
19. Qi, T., Dong, L.J., Qiao, Y., Yu, S.W., Hei, H.J., He, Z.Y., Zhang, Y.X., Jia, Y.X., Zhang, C., Shen, Y.Y.: Enhanced electron field emission of Cu implanted microcrystalline diamond films after annealing. Vacuum **134**, 141–149 (2016)
20. Kumar, I., Khare, A.: Optical nonlinearity in nanostructured carbon thin films fabricated by pulsed laser deposition technique. Thin Solid Films **611**, 56–61 (2016)
21. Petrak, V., Zivcova, Z.V., Krysova, H., Frank, O., Zukal, A., Klimsa, L., Kopecek, J., Taylor, A., Kavan, L., Mortet, V.: Fabrication of porous boron-doped diamond on SiO_2 fiber templates. Carbon **114**, 457–464 (2017)
22. Anwar, M.S., Kumar, S., Arshi, N., Ahmed, F., Seo, Y.J., Lee, C.G., Koo, B.H.: Structural and optical study of samarium doped cerium oxide thin films prepared by electron beam evaporation. J. Alloys Compd. **509**(13), 4525–4529 (2011)
23. Zhang, Z.Y., Huo, F.W., Wu, Y.Q.: Grinding of silicon wafers using an ultrafine diamond wheel of a hybrid bond material. Int. J. Mach. Tools Manuf **51**(1), 18–24 (2011)
24. Zhang, Z.Y., Huo, F.W., Zhang, X.Z., Guo, D.M.: Fabrication and size prediction of crystalline nanoparticles of silicon induced by nanogrinding with ultrafine diamond grits. Scripta Mater. **67**(7–8), 657–660 (2012)
25. Zhang, Z.Y., Huo, Y.X., Guo, D.M.: A model for nanogrinding based on direct evidence of ground chips of silicon wafers. Sci. China Technol. Sci. **56**(9), 2099–2108 (2013)
26. Takagi, M., Onodera, K., Matsumuro, A., Iwata, H., Sasaki, K., Saka, H.: TEM and HRTEM observations of microstructural change of silicon single crystal scratched under very small loading forces by AFM. Mater. Trans. **49**(6), 1298–1302 (2008)
27. Malkin, S., Guo, C.S.: Grinding Technology: Theory and Applications of Machining with Abrasives, Vol. 2 Ch. 2, pp. 14–15. Industrial Press, New York (2008)
28. Zhang, H., Corkhill, C.L., Heath, P.G., Hand, R.J., Stennett, M.C., Hyatt, N.C.: Effect of Zn- and Ca-oxides on the structure and chemical durability of simulant alkali borosilicate glasses for immobilisation of UK high level wastes. J. Nucl. Mater. **462**, 321–328 (2015)
29. Wang, P.F., Li, Z.H., Li, J., Zhu, Y.M.: Effect of ZnO on the interfacial bonding between Na_2O–B_2O_3–SiO_2 vitrified bond and diamond. Solid State Sci. **11**(8), 1427–1432 (2009)
30. Wang, Y.H., Yuan, Y.G., Cheng, X.Z., Li, X.H., Zang, J.B., Lu, J., Yu, Y.Q., Xu, X.P.: Inhibiting the oxidation of diamond during preparing the vitrified dental grinding tools by depositing a ZnO coating using direct urea precipitation method. Mater. Sci. Eng., C **53**, 23–28 (2015)
31. Shen, D.Y., Zhan, Z.L., Liu, Z.D., Cao, Y., Zhou, L., Liu, Y.L., Dai, W., Nishimura, K., Li, C.Y., Lin, C.T., Jiang, N., Yu, J.H.: Enhanced thermal conductivity of epoxy composites filled with silicon carbide nanowires. Sci. Rep. **7**, 2606 (2017)
32. Gopal, A.V., Rao, P.V.: Selection of optimum conditions for maximum material removal rate with surface finish and damage as constraints in SiC grinding. Int. J. Mach. Tools Manuf **43**(13), 1327–1336 (2003)
33. Gopal, A.V., Rao, P.V.: A new chip-thickness model for performance assessment of silicon carbide grinding. Int. J. Adv. Manuf. Technol. **24**(11–12), 816–820 (2004)
34. Fan, S.W., Zhang, L.T., Cheng, L.F., Tian, G.L., Yang, S.J.: Effect of braking pressure and braking speed on the tribological properties of C/SiC aircraft brake materials. Compos. Sci. Technol. **70**(6), 959–965 (2010)
35. Kuo, Y.M., Wang, H.W., Wang, C.T., Tsai, C.H.: Effect of water quenching and SiO2 addition during vitrification of fly ash. Part 1: on the crystalline characteristics of slags. J. Hazard. Mater. **152**(3), 994–1001 (2008)
36. Feng, X.D., Sayle, D.C., Wang, Z.L., Paras, M.S., Santora, B., Sutorik, A.C., Sayle, T.X.T., Yang, Y., Ding, Y., Wang, X.D., Her, Y.S.: Converting ceria polyhedral nanoparticles into single-crystal nanospheres. Science **312**(5779), 1504–1508 (2006)
37. Zhou, L., Eda, H., Shimizu, J., Kamiya, S., Iwase, H., Kimura, S.: Defect-free fabrication for single crystal silicon substrate by chemo-mechanical grinding. CIRP Ann. Manuf. Technol. **55**(1), 313–316 (2006)
38. Pineiro, A., Black, A., Medina, J., Dieguez, E., Parra, V.: The use of potassium peroxidisulphate and Oxone (R) as oxidizers for the chemical mechanical polishing of silicon wafers. Wear **303**(1–2), 446–450 (2013)

39. Rajendran, A., Takahashi, Y., Koyama, M., Kubo, M., Miyamoto, A.: Tight-binding quantum chemical molecular dynamics simulation of mechano-chemical reactions during chemical-mechanical polishing process of SiO_2 surface by CeO_2 particle. Appl. Surf. Sci. **244**(1–4), 34–38 (2005)

40. Hoshino, T., Kurata, Y., Terasaki, Y., Susa, K.: Mechanism of polishing of SiO_2 films by CeO_2 particles. J. Non-Cryst. Solids **283**(1–3), 129–136 (2001)